Contribution from the Institut für anorganische Chemie, Universität Bern, CH-3000 Bern 9, Switzerland, Laboratoire d'Optique Physique, ESPCI, 75231 Paris Cedex 05, France, and Laboratorium für Neutronenstreuung, ETHZ, CH-5303 Würenlingen, Switzerland

Synthesis, Structural Characterization, and Magnetic Properties of V^{3+} Dimer Compounds. Neutron Scattering and Magnetic Circular Dichroism Study of $Cs_3V_2Cl_9$ and $Rb_3V_2Br_9$

Bruno Leuenberger,[†] Bernard Briat,[‡] Jean Claude Canit,[‡] Albert Furrer,[§] Peter Fischer,[§] and Hans U. Güdel*[†]

Received February 10, 1986

The two title compounds were synthesized from a melt and characterized by neutron powder diffraction. The structure is confirmed to be hexagonal, $P6_3/mmc$, with two dimers $V_2X_9^{3-}$ per unit cell. The following lattice parameters were obtained at room temperature: $Cs_3V_2Cl_9$, a = 7.240 (2) Å, c = 17.95 (1) Å; $Rb_3V_2Br_9$, a = 7.361 (2) Å, c = 18.53 (1) Å. The ground-state properties of both V^{3+} compounds were investigated by means of inelastic neutron scattering, magnetic circular dichroism, and magnetic susceptibility measurements. The ground state of V^{3+} is a $^3A_2$ state, and the dimer is described by a spin Hamiltonian containing exchange interaction (J) and zero-field splitting (D) parameters. Both parameters could be determined from the experimental results: $Cs_3V_2Cl_9$, J = 11 cm^{-1}, D = 7.2 cm^{-1}; $Rb_3V_2Br_9$, J = 5.2 cm^{-1}, D = 12 cm^{-1}. Though the exchange interaction is ferromagnetic, the ground level of the dimer is a nonmagnetic singlet. The presence of antiferromagnetic interdimer interactions emerges from our experimental results. Neither compound shows a magnetic ordering above 1.5 K.

Introduction

$Cs_3V_2Cl_9$ and $Rb_3V_2Br_9$ belong to the family of compounds $A_3M_2X_9$ (A = Cs, Rb; M = Ti, V, Cr, Mo, W, Ru; X = Cl, Br).[1-4] The Cr^{3+} compounds crystallize in the hexagonal space group $P6_3/mmc$ with two dimers $M_2X_9^{3-}$ per unit cell. The dimers are oriented along the hexagonal c axis.[3] The symmetry of the dimer is D_{3h}, and the single ion has C_{3v} symmetry. The dimer and the schematic crystal structure are shown in Figure 1. The other members of the above class of compounds are generally believed to be isostructural with the Cr^{3+} compounds. They are thus dimer systems which allow the study of interactions between the two magnetic centers. Of special interest are the $A_3Ti_2X_9$ compounds due to the degenerate ground state of the Ti^{3+} ion. They can therefore be considered as model systems to study exchange interactions between orbitally degenerate ions.[5-7] The Cr^{3+} compounds, on the other hand, have received a great deal of attention as model systems to study exchange interactions in excited states by means of optical spectroscopy.[8-10] Detailed investigation of the Cr^{3+} compounds at low temperatures by use of inelastic neutron scattering spectroscopy showed that interdimer interactions are not negligible. The $A_3Cr_2X_9$ compounds were shown to constitute a novel class of singlet ground-state magnets, namely extended dimerized spin systems.[11,12] The interdimer interaction is strong enough to induce magnetic order at 6.8 K for $Cs_3Cr_2I_9$.[12]

Not much is known about V^{3+} compounds in general.[13-16] V^{3+} has a $^3T_1$ ground state in octahedral coordination that splits into ^3A and ^3E states in axial symmetry. ^3A was found to be the ground state in all V^{3+} compounds studied so far. A zero-field splitting of a few reciprocal centimeters is generally found in this state with the singlet $|10\rangle$ lying below the doublet $|1\pm1\rangle$ in all known compounds.[14] The $A_3V_2X_9$ compounds therefore belong to the interesting class of singlet ground-state magnets. The g values are usually anisotropic with $g_\parallel > g_\perp$. The synthesis of $Cs_3V_2Cl_9$ was described in ref 1, and the lattice constants at room temperature were derived as a = 7.24 Å and c = 17.94 Å. Infrared and diffuse-reflectance spectra of $[Et_2NH_2]_3V_2Cl_9$ were reported in ref 17. No investigation of the magnetic properties of the $A_3V_2X_9$ dimer compounds has been reported up to now.

In the present publication we report the synthesis and structural characterization of $Cs_3V_2Cl_9$ and $Rb_3V_2Br_9$. By use of inelastic neutron scattering (INS) and magnetic circular dichroism (MCD) spectroscopy we investigate the ground state of the $V_2X_9^{3-}$ dimer and determine the exchange interaction and the zero-field splitting parameters.

Experimental Section

The compounds $A_3V_2X_9$ were prepared from stoichiometric mixtures of AX and VX_3 in a melt at 730 °C ($Cs_3V_2Cl_9$) and 700 °C ($Rb_3V_2Br_9$). The reaction time was 5 days. Large single crystals of $Cs_3V_2Cl_9$ were obtained from powdered $Cs_3V_2Cl_9$ at 720 °C by using the Bridgman technique. The powder compounds are very air- and water-sensitive, and all manipulations were performed in a glovebox under dry nitrogen or helium. The details of the synthetic procedure are described elsewhere.[4] The powder samples were checked with X-ray diffraction.

Finely powdered samples of about 5 cm^3 were filled in vanadium cylinders under helium gas for the neutron diffraction experiments. The cylinder was mounted in a closed-cycle refrigerator (T_{min} = 10 K) for the experiments, which were performed on the two-axis spectrometer DMC, which is equipped with a multidetector of 400 counters. The spectrometer is located at the reactor Saphir at Würenlingen, Switzerland. The wavelength of the monochromator was fixed at 1.708 Å, and a 10′ beam collimator was placed in front of the monochromator, together with a cooled Si filter between reactor and monochromator to reduce the epithermic background. The diffraction patterns were measured within a 2θ range of 3-130° and with a step size of 0.1°. The diffraction data were corrected for absorption on the basis of transmission experiments performed on the same spectrometer by using a special transmission setup. Additional neutron diffraction experiments were performed by using a helium gas-flow cryostat (T_{min} = 1.5 K). A standard two-axis spectrometer was used for these experiments. The wavelength of the graphite monochromator was fixed at 2.444 Å.

Powder samples of about 8 cm^3 were filled under helium gas in alu-

[†] Universität Bern.
[‡] Laboratoire d'Optique Physique, ESPCI.
[§] Laboratorium für Neutronenstreuung, ETHZ.

(1) Saillant, R.; Wentworth, R. A. D. *Inorg. Chem.* **1968**, *7*, 1606.
(2) Darriet, J. *Rev. Chim. Miner.* **1981**, *18*, 27.
(3) Saillant, R.; Jackson, R. B.; Streib, W. E.; Folting, K.; Wentworth, R. A. D. *Inorg. Chem.* **1971**, *10*, 1453.
(4) Stebler, A.; Leuenberger, B.; Güdel, H. U. *Inorg. Synth.*, in press.
(5) Briat, B.; Kahn, O.; Morgenstern-Badarau, I.; Rivoal, J. C. *Inorg. Chem.* **1981**, *20*, 4193.
(6) Leuenberger, B.; Güdel, H. U. *Mol. Phys.* **1984**, *51*, 1.
(7) Drillon, M.; Georges, R. *Phys. Rev. B: Condens. Matter* **1982**, *26*, 3882.
(8) Briat, B.; Russel, M. F.; Rivoal, J. C.; Chapelle, J. P.; Kahn, O. *Mol. Phys.* **1977**, *34*, 1357.
(9) Dean, N. J.; Maxwell, K. J.; Stevens, K. W. H.; Turner, R. J. *J. Phys. C* **1985**, *18*, 4505.
(10) Dubicki, L.; Ferguson, J.; Harrowfield, B. V. *Mol. Phys.* **1977**, *34*, 1545.
(11) Leuenberger, B.; Stebler, A.; Güdel, H. U.; Furrer, A.; Feile, R.; Kjems, J. K. *Phys. Rev. B: Condens. Matter* **1984**, *30*, 6300.
(12) Leuenberger, B.; Güdel, H. U.; Fischer, P. *Phys. Rev. B: Condens. Matter*, in press.
(13) Abragam, A.; Bleaney, B. *Electron Paramagnetic Resonance of Transition Ions*; Clarendon: Oxford, 1970; p 426 ff, p 479 ff.
(14) Carlin, R. L.; van Duyneveldt, A. J. *Magnetic Properties of Transition Metal Compounds*; Springer-Verlag: New York, 1977; p 199 ff.
(15) Carlin, R. L.; O'Connor, C. J.; Bhatia, S. N. *Inorg. Chem.* **1976**, *15*, 985.
(16) Smit, J. J.; van Wijk, H. J.; de Jongh, L. J.; Carlin, R. L. *Chem. Phys. Lett.* **1979**, *62*, 158.
(17) Crouch, P. C.; Fowles, G. W. A.; Walton, R. A. *J. Chem. Soc. A* **1969**, 172.

0020-1669/86/1325-2930$01.50/0

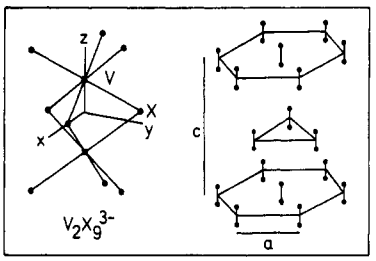

Figure 1. Schematic hexagonal structure of $A_3V_2X_9$ and the dimer $V_2X_9^{3-}$ of D_{3h} symmetry. The dimer coordinate system is included.

minum cylinders for the inelastic neutron scattering experiments. The sample cylinder was placed in a closed-cycle refrigerator (T_{min} = 8 K). The experiments were performed on the triple-axis spectrometer MARC, which is located at the reactor Saphir at Würenlingen, Switzerland. The energy of the analyzer was fixed to 110 cm^{-1}, and the energy of the incoming neutrons was varied. A graphite filter was placed in front of the analyzer to reduce the higher order contributions. A graphite (002) monochromator was used for these experiments. Some high-resolution experiments were performed by using a fixed analyzer energy of 40 cm^{-1} and a beryllium filter in front of the analyzer.

Optical transmission experiments require very thin single crystals (thickness $\simeq 1$ μm) in order to investigate spin-allowed bands in a pure material. Furthermore, the light must propagate along the c axis and the magnetic field B for MCD measurements. These two requirements were easily met in the case of $Cs_3V_2Cl_9$ crystals, which are not very air-sensitive. Just prior to the experiment the crystal was cleaved perpendicular to the c axis. The cleavage plane was then protected by quickly sealing it onto a glass window by means of glycol polyphthalate. The other face was finally ground to an appropriate thickness and polished. The precise thickness was determined by comparing the absorbance of this sample in the near-infrared region with that of the originally cleaved crystal. The same technique was used for $Rb_3V_2Br_9$ under a stream of dry nitrogen, but the material deteriorated significantly during this process. Two series of absorption and MCD experiments were performed on $Cs_3V_2Cl_9$, above 4.2 K with a flow cryostat placed between the poles of an electromagnet (0.7 T) and below 4.2 K in an immersion cryostat containing a superconducting magnet (B_{max} = 2.5 T). The MCD spectrometer incorporates a lock-in phase-sensitive detector and a homemade photoelastic modulator.[18] Absorption spectra were taken with the same instrument.

Powder samples of about 50 mg were filled in Plexiglas containers under helium gas for the magnetic susceptibility measurements. These measurements were performed with the moving-sample technique by using a helium cryostat equipped with a superconducting magnet. The applied magnetic field was chosen to be in the range in which the magnetization depends linearly on the field. The magnetic field was 0.52 and 1.03 T for $Rb_3V_2Br_9$ and $Cs_3V_2Cl_9$, respectively. The data were corrected for diamagnetic contributions, which were estimated to be -377×10^{-6} and -426×10^{-6} emu/mol for $Cs_3V_2Cl_9$ and $Rb_3V_2Br_9$, respectively.[19]

The structure determination was performed on a CDC computer by using a Rietveld program.[20] The following neutron scattering lengths were used (10^{-12} cm): Cs, 0.542; Rb, 0.708; V, −0.038; Cl, 0.958; Br, 0.679.[21]

Theoretical Model

The ground state of V^{3+} is assumed to be the $^3A_2$ state in trigonal symmetry. We can interpret all our results with this assumption (vide infra). The interaction between the two V^{3+} ions is approximated by a Heisenberg Hamiltonian. When the zero-field splitting is taken into account, an appropriate Hamiltonian for the $V_2X_9^{3-}$ dimer in an applied magnetic field is given by

$$H = -J\mathbf{S}_a\cdot\mathbf{S}_b + D((S_a^z)^2 + (S_b^z)^2 - \tfrac{4}{3}) + \mu_b\mathbf{B}\mathbf{g}\mathbf{S}_a + \mu_b\mathbf{B}\mathbf{g}\mathbf{S}_b \quad (1)$$

a and b identify the two V^{3+} ions, and J and D are the exchange and the zero-field splitting parameters, respectively. The g tensor is defined by $g_\parallel$ and $g_\perp$, which represent the g values parallel and perpendicular to the z axis. The coordinate system is included in Figure 1. On each V^{3+} ion we use the $^3A_2$ spin functions as a basis: $|10\rangle$, $|1{-}1\rangle$, and $|1{+}1\rangle$. The basis functions of the dimer $|SM\rangle$ are easily obtained by coupling the two single-ion functions. This leads to singlet, triplet, and quintet dimer basis functions. The calculation of the matrix of the Hamiltonian (1) is straightforward, and its diagonalization leads to the following eigenvalues and functions in the absence of a magnetic field:

$$\begin{aligned} |1\rangle &= -\beta|00\rangle + \alpha|20\rangle & J/2 - D/3 - \epsilon \\ |2\rangle &= |2\pm1\rangle & -J - D/3 \\ |3\rangle &= |2\pm2\rangle & -J + 2D/3 \\ |4\rangle &= |1\pm1\rangle & J - D/3 \\ |5\rangle &= |10\rangle & J + 2D/3 \\ |6\rangle &= \alpha|00\rangle + \beta|20\rangle & J/2 - D/3 + \epsilon \end{aligned} \quad (2)$$

with

$$\epsilon = \tfrac{1}{2}[4D^2 + 9J^2 + 4DJ]^{1/2}$$

$$\alpha = -2(2^{1/2})D/[8D^2 + (9J/2 + D - 3\epsilon)^2]^{1/2} \quad (3)$$

$$\beta = (9J/2 + D - 3\epsilon)/[8D^2 + (9J/2 + D - 3\epsilon)^2]^{1/2}$$

The numbering on the left side of eq 2 will be used to identify the dimer states. Only the dimer basis functions $|00\rangle$ and $|20\rangle$ mix under Hamiltonian (1) in the absence of a magnetic field. The effect of a magnetic field along z is only to split the doublets $|2\pm1\rangle$, $|2\pm2\rangle$, and $|1\pm1\rangle$ by an amount of $2u$, $4u$, and $2u$, respectively, where $u = g_\perp\mu_bB$. For a magnetic field perpendicular to the z direction we used a numerical diagonalization of the Hamiltonian to obtain the eigenvalues. The magnetic susceptibility was obtained by using the Hellman–Feynman theorem.[22,23]

The absorption band under MCD investigation is very broad, and the MCD integrated intensity $\langle\Delta A\rangle_0$ is governed by the difference in population among the two components of individual ground-state doublets. Actually, since the MCD line shape is not significantly modified in the investigated temperature range, we can as well use the maximum of ΔA as the appropriate variable instead of the zero-order moment $\langle\Delta A\rangle_0$. Let us consider for example the doublet $|2\rangle = |2\pm1\rangle$ and let A_2^+ and A_2^- be the integrated intensities of left and right polarized absorption originating from the $M = -1$ Zeeman sublevel. With $A_2 = A_2^+ - A_2^-$, the MCD contribution from this doublet will be

$$\Delta A_2 = p_2A_2(e^y - e^{-y}) \quad (4)$$

with

$$y = g_\parallel\mu_bB/kT$$

p_i is the population factor of the level $|i\rangle$ whose energy E_i in zero external field is defined in eq 2. Formula 4 also applies to the $|1\pm1\rangle$ level (ΔA_4) with p_4A_4 instead of p_2A_2. By contrast, ΔA_3 will show a different field and temperature dependency:

$$\Delta A_3 = p_3A_3(e^{2y} - e^{-2y}) \quad (5)$$

A priori, A_2, A_3, and A_4 can be positive or negative. With the same formalism and in zero magnetic field, the total integrated absorption intensity from the ground-state manifold is given by

$$A = p_1A_1^+ + p_5A_5^+ + p_6A_6^+ + p_2(A_2^+ + A_2^-) + p_3(A_3^+ + A_3^-) + p_4(A_4^+ + A_4^-) \quad (6)$$

The theory for the INS intensity calculation is outlined in ref 24. It leads to the selection rules

$$\Delta S = 0, \pm1 \qquad \Delta M = 0, \pm1 \quad (7)$$

The mixing of the $|00\rangle$ and $|20\rangle$ functions must be taken into account when eq 7 is used.

Results

(a) Structural Characterization. The original reason for performing elastic neutron scattering experiments on the $A_3V_2X_9$ compounds was to look for a possible magnetic order at low temperatures. First, however, we had to determine the nuclear structure at room temperature.

The neutron diffraction patterns of $Cs_3V_2Cl_9$ and $Rb_3V_2Br_9$ are shown in Figure 2. A Rietveld analysis in the hexagonal space group $P6_3/mmc$ was performed with these data. The initial atomic positions were taken from the analogous $Cs_3Cr_2X_9$ compounds.[3] The background was determined for 15 points, linearly interpolated, and subtracted from the measured profile. It was not refined

(18) Canit, J. C.; Badoz, J. *Appl. Opt.* **1984**, *23*, 2861.
(19) Landolt-Börnstein, *Physikalische und Chemische Tabellen*; Springer-Verlag: West Berlin, 1976; Neue Serie II/8, p 27.
(20) Rietveld, H. M. *J. Appl. Crystallogr.* **1969**, *2*, 65.
(21) Sears, V. F. *At. Energy Can. Ltd.*, [*Rep.*] *AECL* **1984**, *AECL*-8490, 16.
(22) Leuenberger, B. Lizentiatsarbeit, University of Bern, 1982.
(23) Gregson, A. K. *Aust. J. Chem.* **1980**, *33*, 2574.
(24) Stebler, A.; Güdel, H. U.; Furrer, A.; Kjems, J. K. *Inorg. Chem.* **1982**, *21*, 380.

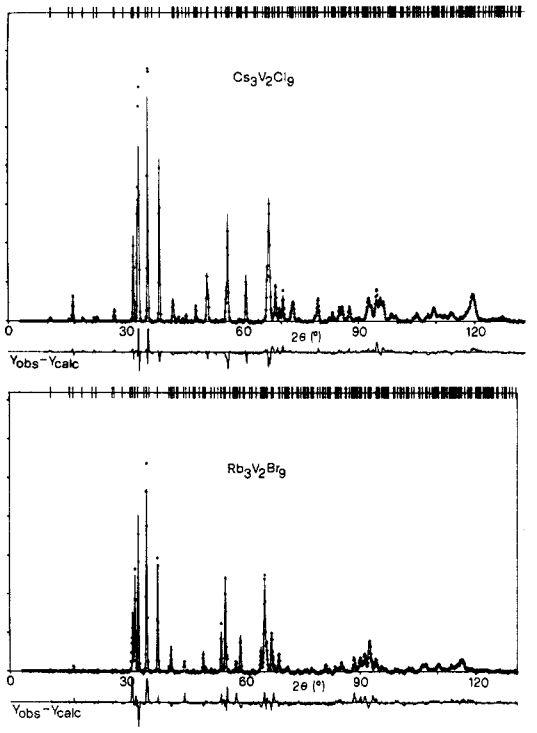

Figure 2. Rietveld analysis of the neutron diffraction patterns of $Cs_3V_2Cl_9$ and $Rb_3V_2Br_9$ at room temperature. The wavelength was 1.708 Å. The squares correspond to the observed intensities, and the solid line represents the Rietveld fit. The tic marks on the top show the individual Bragg reflections.

Table I. Structural Parameters of $Cs_3V_2Cl_9$ and $Rb_3V_2Br_9$ at Room Temperature Obtained from a Rietveld Analysis of Powder Neutron Diffraction Data[a]

	$A_3V_2X_9$	
	$Cs_3V_2Cl_9$	$Rb_3V_2Br_9$
a, Å	7.240 (2)	7.361 (2)
c, Å	17.95 (1)	18.53 (1)
a(10, 1.5 K), Å	7.18 (2)	7.297 (2)
c(10, 1.5 K), Å	17.8 (1)	18.34 (1)
vol, Å^3	814.8 (2)	869.8 (3)
mol wt, g/mol	819.66	1077.48
(4e) A (0, 0, $^1/_4$)		
(4f) A ($^1/_3$, $^2/_3$, z): z	0.0763 (9)	0.0715 (9)
(4f) V ($^1/_3$, $^2/_3$, z): z	0.8380[b]	0.8388[b]
(6h) X (x, $2x$, $^1/_4$): x	−0.4833 (6)	−0.4904 (15)
(12h) X (x, $2x$, z): x, z	−0.1765 (4), 0.0919 (3)	−0.1681 (4), 0.0884 (4)
temp factor, Å^2	1.9 (2)	2.6 (2)
R_I	0.153	0.214
R_{wp}	0.203	0.296
R_p	0.211	0.261

[a] The R values are defined in ref 25. The space group is $P6_3/mmc$ with $Z = 2$. [b] Fixed to the value of the analogous $Cs_3Cr_2X_9$ (X = Cl, Br) compounds.

in the Rietveld fit. In addition to the atomic positional parameters we refined the lattice constants, the zero point of the detector, the overall scale factor, and three half-width parameters of the Gaussian line shapes as defined in ref 20. It was found unnecessary to introduce a parameter for preferred orientation. The determined lattice and atomic parameters are summarized in Table I, and the result of the fit is included in Figure 2. Due to the negligible nuclear scattering length of V, it was not possible to refine the position of this atom. Its position was kept fixed at the value of the analogous Cr^{3+} compound. We obtained integral R_I values of 0.153 and 0.214 for $Cs_3V_2Cl_9$ and $Rb_3V_2Br_9$, respectively. The R values are defined in ref 25. They are relatively large, which we attribute to the presence of small amounts of unidentified impurities, which are inevitably present in samples of this type. The larger R value of the bromide compound with respect to that of the chloride reflects its increased air and water sensitivity. Our structural characterization does not represent a detailed structure determination. But it strongly indicates that the two V^{3+} compounds are isostructural with $Cs_3Cr_2Cl_9$. On the basis of the analogy with the Cr^{3+} compounds $Cs_3Cr_2X_9$, X = Cl, Br,[3] the separation between the V^{3+} ions within a dimer is estimated as 3.16 Å for $Cs_3V_2Cl_9$ and 3.29 Å for $Rb_3V_2Br_9$. Included in Table I are the lattice constants at low temperatures (10, 1.5 K). Those of $Rb_3V_2Br_9$ have smaller standard deviations because they were obtained from a Rietveld fit of a measured diffraction diagram at 10 K, whereas those of $Cs_3V_2Cl_9$ were obtained from the positions of 10 reflections. The atomic positional parameters of $Rb_3V_2Br_9$ at 10 K were found to be essentially equal to those at room temperature.

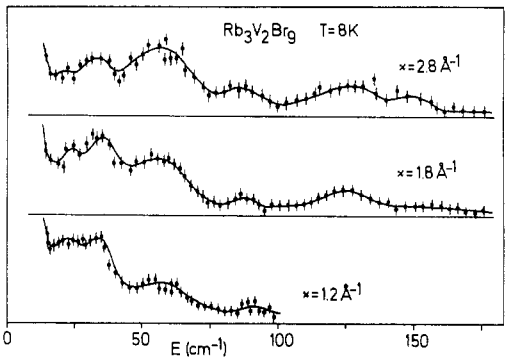

Figure 3. Inelastic neutron scattering spectra of $Rb_3V_2Br_9$ at 8 K for various scattering vectors. The solid lines are guides to the eye.

Elastic neutron scattering experiments were performed down to 1.5 K with both compounds. No evidence for magnetic order was found for either compound. In addition, our experiments showed no evidence for structural phase transitions.

(b) Inelastic Neutron Scattering. Figure 3 shows inelastic neutron scattering spectra of $Rb_3V_2Br_9$ at 8 K for several scattering vectors κ. The intensities of the two bands at 18 and 31 cm^{-1} decrease with increasing scattering vector. This is typical for magnetic excitations. The decrease of the intensity is due to the rapidly decreasing form factor with increasing scattering vector.[24] On the other hand, the intensity of the high-energy bands increases with increasing scattering vector. This is the typical behavior of phonon scattering. The intensity as a function of κ was thus used to distinguish between electronic and vibrational transitions. In addition, the temperature dependence of the intensity was used to identify electronic transitions which follow Boltzmann statistics. On the basis of these arguments we identified the two lowest transitions at energies of 18 and 31 cm^{-1} in Figure 3 as electronic. All the other bands in Figure 3 are of vibrational origin. We measured the spectrum up to an energy transfer of 570 cm^{-1} and found no additional electronic bands. This indicates that the ^3E state is more than 570 cm^{-1} above the $^3A_2$ ground state. The half-widths of the electronic bands are about 7 cm^{-1}, while the resolution of the spectrometer is 5.5 cm^{-1}. This indicates that the electronic bands are broadened by some physical effect. Interdimer interactions are likely to be responsible for the broadening in this case. They lead to an energy dispersion of the dimer excitations. Powder measurements produce an averaged spectrum over this dispersion and therefore lead to broadened bands. To investigate this in more detail and also to look for a third electronic transition below 15 cm^{-1}, we performed measurements with higher resolution. Figure 4 shows the high-resolution spectrum. A third electronic transition around 10 cm^{-1} just barely emerges from the background. This transition was masked in the spectra of Figure 3 by the quasi-elastic line due to the poorer resolution. The resolution of the spectrometer was 0.8 cm^{-1} in the experiments of Figure 4. The electronic bands are significantly broader, namely 4 cm^{-1}. This clearly indicates that interdimer interaction is present and broadens the magnetic excitations.

(25) Malmros, G.; Thomas, J. O. *J. Appl. Crystallogr.* **1977**, *10*, 7.

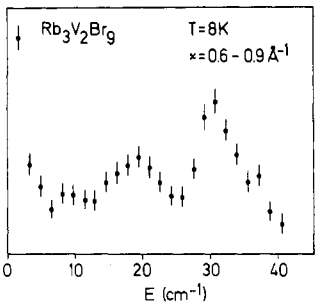

Figure 4. High-resolution neutron scattering spectrum of $Rb_3V_2Br_9$ at 8 K obtained by averaging four measurements in the κ range 0.6–0.9 Å^{-1} to improve the statistics.

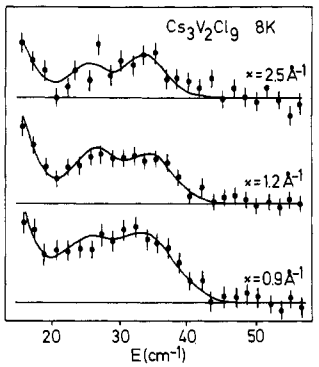

Figure 5. Inelastic neutron scattering spectra of $Cs_3V_2Cl_9$ at 8 K for various scattering vectors. The solid lines correspond to fits with Gaussians.

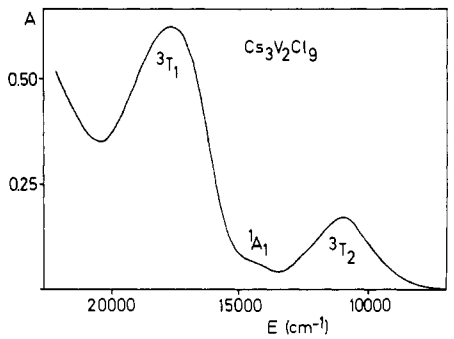

Figure 6. Axial absorption spectrum of $Cs_3V_2Cl_9$ at room temperature. The absorbance A is given for a crystal with a thickness of 1 μm.

Figure 5 shows INS spectra of $Cs_3V_2Cl_9$ at 8 K for several scattering vectors. We can identify two electronic transitions at approximately 26 and 34 cm^{-1}. The intensities of both bands decrease with increasing scattering vector, as expected for magnetic excitations. The resolution of the spectrometer was 5.5 cm^{-1}, and the half-widths of the transitions are about 7 cm^{-1}. Interdimer interactions appear to broaden the powder bands also in $Cs_3V_2Cl_9$.

To conclude, the INS experiments show three electronic transitions for $Rb_3V_2Br_9$ at 10, 18, and 32 cm^{-1}, and two for $Cs_3V_2Cl_9$ at 26 and 34 cm^{-1}. It is not possible to identify the symmetry of these states according to the theory outlined in ref 24, because the statistics of the data are not good enough and interdimer interactions broaden the bands.

(c) Absorption and MCD Spectra. Figure 6 shows an overview of the axial absorption spectrum of $Cs_3V_2Cl_9$ at room temperature. The two main bands result from the spin-allowed d–d transitions to the $^3T_2$ and $^3T_1$ excited states. Figure 7 shows the absorption and MCD spectra of $Cs_3V_2Cl_9$ in the $^3T_1$ region for various temperatures. Three peaks or shoulders are clearly observed around 17 300, 18 100, and 18 700 cm^{-1} in the two spectra. Only minor changes were found to occur in the absorption spectrum upon cooling from 300 to 1.7 K. This indicates that the various terms A_i^+ in eq 6 have approximately the same magnitude. It also confirms our conclusion from INS that the ^3E component of the ground-state manifold lies more than 570 cm^{-1} above $^3A_2$ and is not thermally populated at 300 K. The strong temperature dependence of the MCD was studied in great detail between 65 and 1.7 K. It was found to be the same for two crystals grown independently in Bern and Paris. The result of these measurements is summarized in Figure 8. The field dependence of ΔA was also investigated at 1.7 and 4.2 K and is shown in Figure 9. Three weak MCD features were clearly observed in the $^1A_1$ region at 14 300, 15 400, and 15 900 cm^{-1}. They are about 250 times less intense than ΔA for the major band, and they are not reported in Figure 7.

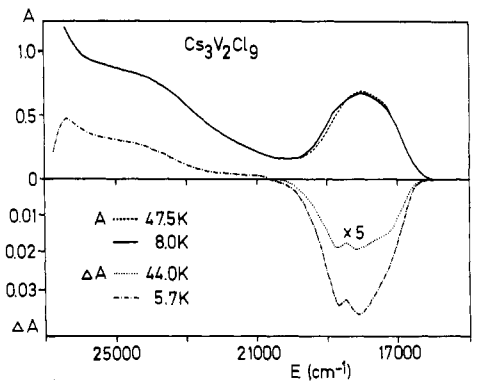

Figure 7. Axial absorption and MCD spectra of $Cs_3V_2Cl_9$ at various temperatures. The magnetic field of 0.7 T was applied in the c direction of the hexagonal lattice. Note that the MCD around 18 000 cm^{-1} is positive and that the spectrum at 44 K has been magnified 5 times.

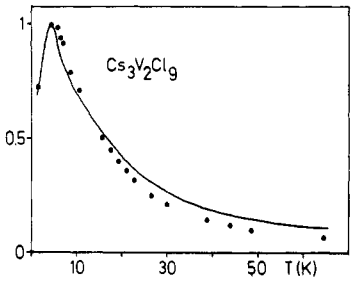

Figure 8. Temperature dependence of the MCD intensity (normalized to 1 at 4.2 K) of $Cs_3V_2Cl_9$ at a field of 0.7 T. The points represent the experimental values, and the curve was calculated with the parameters of Table II by using eq 4 and 5 and with $A_2 = A_3 = -A_4$ and $g_\parallel = 1.9$.

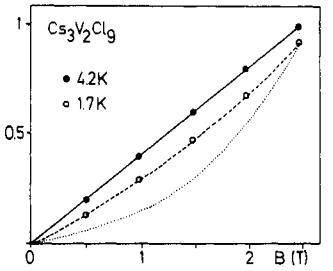

Figure 9. Magnetic field dependence of the MCD intensity of $Cs_3V_2Cl_9$ at 1.7 and 4.2 K (normalized to 1 at 4.2 K and 2.5 T). The points represent the experimental values. The solid and the dashed lines were calculated with eq 4 (MCD for a $|S'\pm1\rangle$ first excited level), while the dotted line was obtained by using eq 5 (MCD for the $|2\pm2\rangle$ first excited level).

The temperature dependence of the MCD in Figure 8 demonstrates very clearly that the ground level of the dimer is a nonmagnetic singlet and that there is a magnetic level at only slightly higher energy. An analysis of our data obtained at 4.2 and 1.7 K with a simple two-level model with a ground level $|S0\rangle$ and a low-lying level $|S'\pm1\rangle$ indicates that the energy difference between these levels is 3.4 (1) cm^{-1} if we assume $g_\parallel = 1.9$. Choosing $g_\parallel = 1.6$ changes this energy to 3.8 cm^{-1}. The possibility that the first excited level is $|2\pm2\rangle$ can be ruled out absolutely on the basis of the field dependence of ΔA in Figure 9. The dotted

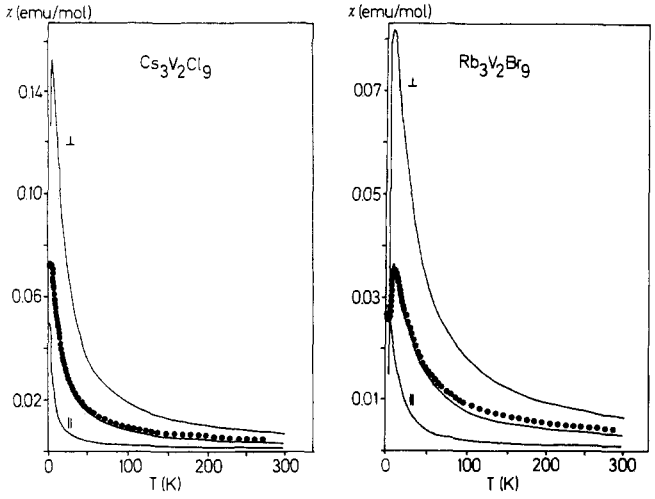

Figure 10. Magnetic powder susceptibility of $Cs_3V_2Cl_9$ and $Rb_3V_2Br_9$. The points represent the experimental data, and the curves were fitted according to eq 3. The labels ⊥ and ∥ identify the susceptibilities perpendicular and parallel to the hexagonal c axis.

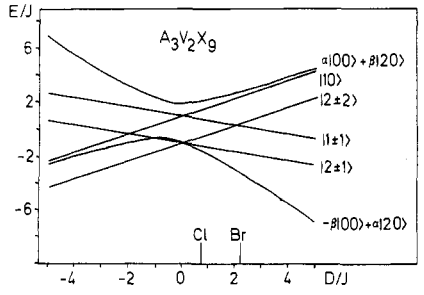

Figure 11. Energy level diagram of E/J as a function of D/J for $A_3V_2X_9$ according to eq 2. The D/J values of $Cs_3V_2Cl_9$ and $Rb_3V_2Br_9$ are indicated.

line corresponds to a calculation using a two-level model with $|2\pm2\rangle$ as the upper level. It is at variance with the data. This analysis is essentially independent of additional levels at higher energies and the precise value of A_2 in eq 4. Considering our MCD data between 4.4 and 9 K then leads to the unambiguous conclusion that the $|2\pm2\rangle$ doublet lies at 10.0 (5) cm^{-1}. A_2 and A_3 are both positive, and we have assumed that $A_2 \simeq A_3$.

To summarize, the MCD experiments on $Cs_3V_2Cl_9$ identify the ground level of the dimer as a nonmagnetic singlet and show that the first two excited levels are $|S'\pm1\rangle$ and $|2\pm2\rangle$ doublets lying 3.4 and 10 cm^{-1}, respectively, above the ground level. It is not possible to reproduce the high-temperature region with this three-level model. This indicates that there are additional levels at higher energies, as expected.

(d) Magnetic Susceptibilities. Figure 10 shows the magnetic powder susceptibilities of $Cs_3V_2Cl_9$ and $Rb_3V_2Br_9$ between 1.5 K and room temperature. The data of $Rb_3V_2Br_9$ show a maximum at 12 K. The decrease at lower temperatures results from the nonmagnetic ground level and the maximum from an excited magnetic level. The very small increase of the susceptibility at the lowest temperatures is due to paramagnetic impurities. An analogous maximum in the magnetic susceptibility of $Cs_3V_2Cl_9$ is indicated by the three lowest data points. It thus occurs at lower temperature than in $Rb_3V_2Br_9$. We conclude that the first excited magnetic level lies at higher energy in the bromide than in the chloride.

Analysis

Our main aim was the determination of the zero-field splitting parameter D and the exchange parameter J for $Cs_3V_2Cl_9$ and $Rb_3V_2Br_9$. The energy level pattern represented by eq 2 is shown in Figure 11, where the energies of the levels E/J are plotted as a function of D/J. We first consider an antiferromagnetic exchange, i.e. a negative J value. From Figure 11 we see that the ground level is a nonmagnetic singlet, $\alpha|00\rangle + \beta|20\rangle$, for this case. A negative D value leads to a first excited level, which is nonmagnetic. This possibility is ruled out for $Cs_3V_2Cl_9$ by our MCD result, which clearly identified the first excited level as a magnetic $|S'\pm1\rangle$ level. It is also unlikely for $Rb_3V_2Br_9$ on the basis of the magnetic susceptibility. A positive D value, on the other hand, would lead to a magnetic first excited level, namely to $|1\pm1\rangle$, quite consistent with our MCD results. It turns out, however, that the second excited level in this situation can by no means be $|2\pm2\rangle$, as determined by MCD. Considering now the INS, three transitions are allowed to the levels $|1\pm1\rangle$, $|10\rangle$, and $|2\pm1\rangle$ for this situation. This is in qualitative agreement with the INS experiments. However, for $Cs_3V_2Cl_9$ we observed two transitions around 26 and 32 cm^{-1}, and the MCD experiment identified a third magnetic level, $|S'\pm1\rangle$, at 3.4 cm^{-1}. Figure 11 shows that it is not possible to reproduce such a splitting pattern assuming a negative J value. The possibility of an antiferromagnetic J and a positive D is therefore ruled out on the basis of both MCD and INS experiments.

We now consider a ferromagnetic exchange, i.e. a positive J value. For a negative D we obtain a magnetic ground level, in contradiction with all the experimental evidence. A positive D value, on the other hand, leads to the nonmagnetic ground level $-\beta|00\rangle + \alpha|20\rangle$ followed by the first magnetic level $|2\pm1\rangle$. The energy separations in Figure 11 indicate that this possibility could fit our spectroscopic data. Moreover, we conclude that $D/J < 2$ for $Cs_3V_2Cl_9$, since $|2\pm2\rangle$ is the second excited level.

On the basis of these qualitative arguments we proceeded to a quantitative determination of J and D by fitting the INS transition energies and, for $Cs_3V_2Cl_9$, the two energies of 3.4 and 10 cm^{-1}, which were obtained from the MCD study. The MCD was calculated as a function of temperature according to eq 4 and 5 and with $A_2 = A_3 = -A_4$. This procedure confirmed that for both $Cs_3V_2Cl_9$ and $Rb_3V_2Br_9$ only a ferromagnetic J and a positive D value can explain all our data. The obtained J and D values are collected in Table II. Calculated and observed energies are also included in Table II. The overall agreement is good. The calculated MCD as a function of temperature and magnetic field is compared with the experimental data in Figures 8 and 9. Also here the agreement is good. The deviations in Figure 8 are thought to be due to three factors. The three parameters A_2, A_3, and A_4 probably do not have exactly the same value and interdimer interactions have been neglected. In addition, the ground state $^3A_2$ of the single ion in trigonal symmetry is significantly mixed to ^3E via spin–orbit coupling.

Our model contains as additional parameters the two g values $g_\parallel$ and $g_\perp$. They were obtained by a least-squares fit of the calculated susceptibility according to the Hamiltonian (1) to the experimental data. The values of J and D were kept fixed for this fit. The results are shown in Figure 10. An introduction of a temperature-independent paramagnetism did not lead to a better fit. The following g values were obtained from the fit: $Cs_3V_2Cl_9$,

Table II. Parameter Values of $Cs_3V_2Cl_9$ and $Rb_3V_2Br_9$ As Defined in Eq 2[a]

params	$Cs_3V_2Cl_9$	$Rb_3V_2Br_9$
J, cm^{-1}	11	5.2
D, cm^{-1}	7.2	12
α	−0.986	−0.928
β	−0.167	−0.373

	energies, cm^{-1}			
	$Cs_3V_2Cl_9$		$Rb_3V_2Br_2$	
	calcd	obsd	calcd	obsd
$-\beta\|00\rangle + \alpha\|20\rangle$				
$\|2\pm1\rangle$ INS	3.5	3.4 (MCD)	8.5	≃10 (INS)
$\|1\pm1\rangle$ INS	26.3	26 (INS)	18.9	18 (INS)
$\|2\pm2\rangle$	10.7	10 (MCD)	20.5	
$\|10\rangle$ INS	33.5	34 (INS)	30.9	31 (INS)
$\alpha\|00\rangle + \beta\|20\rangle$	41.3		32.7	

[a] The observed and calculated energies are also included. The allowed transitions for inelastic neutron scattering are indicated by INS.

$g_\parallel = 1.8$, $g_\perp = 0.43$; $Rb_3V_2Br_9$, $g_\parallel = 1.9$, $g_\perp = 0.44$. For $Cs_3VCl_6 \cdot 4H_2O$ the g values have been determined to be $g_\parallel = 1.93$ and $g_\perp = 1.74$ from EPR experiments.[15,16] Our $g_\parallel$ values seem quite reasonable. This is not the case for $g_\perp$, for which we obtained very low values. The origin of these low $g_\perp$ values is not completely clear. It is generally difficult to obtain good g values from susceptibility data if J and D are taken from independent experiments. The large anisotropy of the g values could, partially, result from a preferred orientation of crystallites in the powder samples. The large reduction of $g_\perp$, on the other hand, could partially originate from antiferromagnetic interdimer interactions, which generally lead to a reduction of the g values. The ^3E state, which has been neglected, also affects the g values. The contamination of the ground-state wave functions by the ^3E state will primarily affect the wave functions and therefore the g values but not the energies.

The INS intensities can be calculated according to the theory outlined in ref 24. Transitions originating in excited levels are included in the calculation with the appropriate population factors. For $Cs_3V_2Cl_9$ the two observed transitions have approximately equal intensity, in reasonable agreement with the calculation, which predicts an intensity ratio of 1.2. For $Rb_3V_2Br_9$ the observed intensity ratios for the three transitions at 10, 18, and 31 cm^{-1} are approximately 0.7/1/1.2 and the calculation leads to a ratio of 1.3/1/0.2 for $\kappa = 1$ $Å^{-1}$. The rather poor agreement is attributed to the same factors that are responsible for the discrepancies of g values, as discussed in the previous paragraph. In addition, the observed intensities are only semiquantitative due to the moderate statistics of the experimental data.

Discussion

For both $Cs_3V_2Cl_9$ and $Rb_3V_2Br_9$ we obtain positive D values as is the case for all known V^{3+} compounds.[14] The determined D values of 7.2 and 12 cm^{-1} for $Cs_3V_2Cl_9$ and $Rb_3V_2Br_9$, respectively, are of the same order of magnitude as the value $D = 8.05$ cm^{-1} obtained for $Cs_3VCl_6 \cdot 4H_2O$.[15,16]

From the widths of the INS transitions we argued that interdimer interactions are present in $A_3V_2X_9$. The analysis of the susceptibility data indicates that the interdimer interaction is antiferromagnetic, as is the case for the analogous Cr^{3+} compounds.[11,26]

The most interesting result of our study is certainly the ferromagnetic intradimer interaction J, which requires some comment. The intradimer exchange is antiferromagnetic for the analogous compounds $Cs_3Cr_2Cl_9$ and $Cs_3Cr_2Br_9$. The J values can generally be decomposed into a ferromagnetic part J_f and an antiferromagnetic part J_{af}:

$$J = J_{af} + J_f \quad (8)$$

The antiferromagnetic part can be related to energy differences between dimer orbitals. This decomposition depends on the electron configuration and is different for the Cr^{3+} and V^{3+} compounds:[26,27]

$$Cr^{3+}: \; J_{af} = -\tfrac{1}{9}(J_a + 2J_e) \qquad V^{3+}: \; J_{af} = -\tfrac{1}{2}J_e \quad (9)$$

J_a and J_e are parameters related to single-ion orbitals of symmetry a_1 and e, respectively, in C_{3v}. They are defined and discussed in ref 26 and 27. In ref 27 it was shown that J_a dominates J_e. The ratio J_a/J_e was estimated to be 17 for $V_2Cl_9^{3-}$ and to be 18 for $Cr_2Cl_9^{3-}$.[27] In addition it was found that J_a varies more than J_e when Cl is replaced by Br.[26] From eq 9 we therefore expect that $|J_{af}(Cr_2Cl_9^{3-})| > |J_{af}(V_2Cl_9^{3-})|$. The J values of $Cr_2Cl_9^{3-}$ and $Cr_2Br_9^{3-}$ were determined to be -8.3 and -14.1 cm^{-1}, respectively.[11,26] These values are already quite small. J_{af} for the V^{3+} compounds is expected to be even significantly smaller because there is no contribution from J_a. J_{af} thus becomes so small that J_f dominates and determines the sign of J. J_f in eq 9 is more difficult to estimate than J_{af}. J_f is essentially an exchange integral and is thus expected to decrease with increasing V–V separation. The chloride compound has a smaller V–V separation (3.16 Å) than the bromide (3.29 Å), and the J value of $Cs_3V_2Cl_9$ is indeed larger than that of $Rb_3V_2Br_9$, in agreement with the expected trend.

The large amount of work which has been done on $Cs_3Cr_2Cl_9$, $Cs_3Cr_2Br_9$, and $Cs_3Cr_2I_9$ and which has shown that these systems have a number of novel and unique properties[11,12,26] suggests additional experiments on the V^{3+} compounds. The compounds $A_3V_2X_9$ may be especially interesting because they show a ferromagnetic intradimer interaction. The large zero-field splitting provides additional richness. In contrast to the Cr^{3+} compounds, where the zero-field splitting is negligibly small, we have a situation where zero-field splitting and exchange interaction are of equal magnitudes. The situation is no longer purely isotropic as in $Cs_3Cr_2X_9$. Inelastic neutron scattering experiments on single crystals of $A_3V_2X_9$ would be highly desirable to study the spin dynamics in the disordered phase and to estimate possible perturbations that could induce magnetic order.

Acknowledgment. We wish to thank K. Mattenberger for performing the susceptibility measurements. Financial support by the Swiss National Science Foundation and the French CNRS is gratefully acknowledged.

Registry No. $Cs_3V_2Cl_9$, 12052-07-2; $Rb_3V_2Br_9$, 102682-48-4.

(26) Leuenberger, B.; Güdel, H. U.; Kjems, J. K.; Petitgrand, D. *Inorg. Chem.* **1985**, *24*, 1035.

(27) Leuenberger, B.; Güdel, H. U. *Inorg. Chem.* **1986**, *25*, 181.